Uniaxial stress and ultrasonic anisotropy in a layered orthorhombic medium

Bode Omoboya (University of Houston), J.J.S de Figueiredo (Unicamp-Brazil and University of Houston), Nikolay Dyaur (University of Houston) and Robert R. Stewart (University of Houston)*

Summary

Studies of orthorhombic anisotropy are becoming progressively essential, especially as many sedimentary rocks are considered to have orthorhombic symmetry. To study the effect of stress in a layered orthorhombic medium, a physical modeling study using intrinsically orthorhombic phenolic boards was conducted. The experiment was designed to simulate sedimentary reservoir rocks deposited in layers with inherent orthotropic symmetry and under the influence of stress due to overlying sediments. The study also explores which geologic phenomena dominate the contortion of anisotropy under different stress tenure. The phenolic boards were coupled together with the help of a pressure device and uniaxial stress was gradually increased while time arrival and velocity measurements were repeated. Results show maximum increase in compressional and shear wave velocities ranging from 4% to 10% in different directions as a function of increasing uniaxial stress. P and S wave dependent stiffness coefficients generally increased with stress. Anisotropic parameters (extension of Thomsen's parameters for orthorhombic symmetry) generally diminished or remained constant with increasing pressure and changes ranged from 0% to 33%. We observed anisotropic behavior a priori to both orthorhombic and VTI symmetries in different principal axes of the model. Polar anisotropy behavior is due primarily to layering or stratification and tends to increase with pressure. Certain anisotropic parameters however unveil inherent orthotropic symmetry of the composite model.

Introduction

A combination of parallel vertical fractures due to regional stress and a background horizontal layering would combine to form orthorhombic symmetry. Due to fact that these two geologic phenomena (horizontal layering/stratification and regional stress) are widespread, orthorhombic symmetry may be a truly realistic anisotropic earth model for reservoir characterization. This paper considers the effect of simulated overburden pressure on phase velocity, stiffness coefficients and anisotropic parameters in a layered orthorhombic medium. The layered medium consists of 55 1.5mm thick phenolic slabs or boards coupled together with a pressure apparatus. Figure 1 is a snapshot of the composite model showing all dimensions and principal directions. Phenolic CE is an industrial laminate with intrinsic orthorhombic symmetry**.**

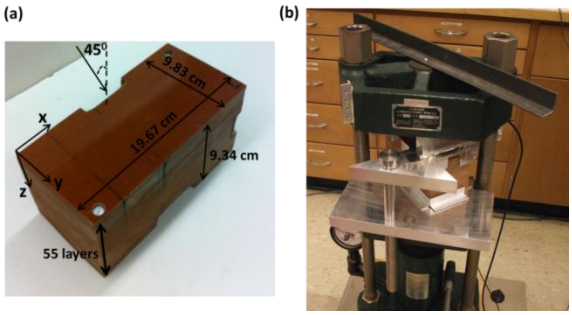

Figure 1: Snapshot of physical model and experimental setup, (a) Phenolic model showing all principal directions (b) AGL designed pressure apparatus with phenolic model embedded

Scaled ultrasonic seismic measurements were taken in radial, sagittal and traverse directions on all block faces, travel times were picked directly from a digital oscilloscope and inverted for compressional and shear wave velocities as well as anisotropic parameters. Uniaxial stress was gradually increased and all measurements were repeated. The experiment was designed to simulate earth-like intrinsically anisotropic rocks buried in layers and so under the influence of pressure from overburden sediments. Previous measurements by Pervukhina and Dewhurst (2008) showed the relationship between anisotropic parameters and mean effective stress in transversely isotropic shale core samples. In this experiment, we extend a similar approach to a physical model of orthotropic symmetry. In a seismic physical modeling experiment, an attempt is made at estimating the seismic response of a geologic model by measuring the reflected or transmitted wave field over the scaled model (Ebrom and McDonald, 1994). The scaling is on travel time and consequently wavelength but all other wave attributes such as velocity remain intact. In physical modeling, it is assumed with a fair degree of accuracy that the physics of elastic wave propagation in the physical model is the same as the real world. This could be explained by infinitesimal strain elastic wave theory (Ebrom and McDonald, 1994). The main objectives of this experiment are as follows:

1) To explore the effect of stress on anisotropy in an inherently anisotropic medium.

2) To explore which physical phenomena (horizontal layering/stratification or vertical fractures) dominates the character of anisotropy as uniaxial stress increases. Our results show anisotropic behavior ascribable to both orthorhombic symmetry and VTI symmetry due to

layering. Anisotropic behavior attributable to polar anisotropy tends to increase with increasing uniaxial stress

Experimental Set-up

The 55 phenolic boards were bound together by an AGL fabricated pressure device connected to pressure and strain gauges. Figure 2 is a schematic of the experimental setup. The principal axes of the composite model are labelled X, Y and Z; with Z being the direction perpendicular to layering (or sedimentation/stratification in a real earth case). The Z direction is also the direction of much interest to exploration geophysics. In comparison to other orthorhombic anisotropy publications, (some publications label principal axes as 1, 2 and 3 axes) X=1, Y=2 and Z=3. The thickness of the phenolic boards ranged from 1.4 mm to 1.7 mm. Before the commencement of travel time measurements, density measurements were taken and a strain test was conducted mainly to test the elastic strength of the composite model. Figure 3 shows a stress strain curve for the model. Uniaxial stress was increased from 0.05MPa to 0.5MPa; in all, 7 sets of measurements were taken. 100 kHz compressional and shear transducers were used to ensure seismic wavelength was at least 10 times the thickness of each phenolic sheet

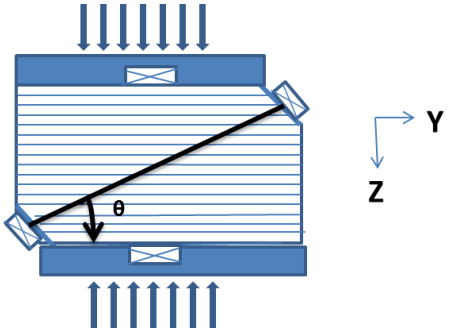

Figure 2: Schematic of experimental setup showing direction of application of stress and position of ultrasonic transducers. **θ** is the phase (wavefront) angle and it differs in different axes because the composite model is a cuboid (45^0 in ZY, 25.4^0 in ZX and 26.6^0 in XY)

The wavelength of compressional wave was measured at ~30 mm (thickness of phenolic board ~1.5 mm). In all measurements (both compressional and shear wave), $\lambda \gg H$ (λ is seismic wavelength and H is thickness of phenolic board). This was to ensure an effective seismic response from the whole model rather than scattering between layers. The source and receiver transducers were placed on opposing sides for a pulse transmission measurement. The direction of polarization of the shear transducer was varied from 0^0 to 180^0 and measurements were taken every 10^0 interval. In each case, 0^0 was shear polarization parallel to bedding plane and 90^0 was polarization perpendicular to bedding plane. Compressional and shear wave arrivals were picked directly from seismograms produced by the AGL scaled ultrasonic system with accuracy of ± 0.1μs. In this experiment, travel time measurements were inverted for phase velocities, this is because the transducers are relatively wide compared to the thickness of the model being measured (Dellinger and Vernik, 1994) .The diameter of the transducers used (both compressional and shear) is 4cm. Transducer response has also been well studied for directivity and delay time. Time arrival measurements were taken in 3 principal axes, Z (3), X (1) and Y (2). Diagonal phase velocity measurements were also taken at 45^0 in ZY axes and at two other oblique angles; 25.4^0 in ZX and 26.6^0 in XY, this is due to the fact that the composite model is a cuboid (Figure 1a). The dimension of the model is; 19.67 cm X 9.83 cm X 9.34 cm. As a result, angle dependent velocities were used across ZX and XY axes to obtain diagonal stiffness coefficients (C_{12} *and* C_{23}). Signal scaling factor is 1:10000. All model construction as well as ultrasonic measurements were carried out at the Allied Geophysical Laboratories (AGL) at the University of Houston.

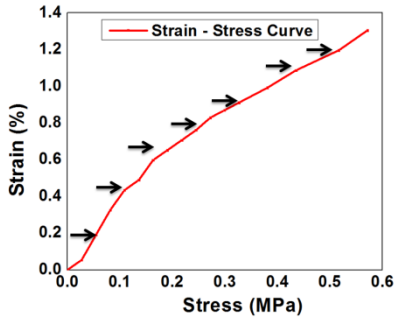

Figure 3: Stress-Strain curve for layered phenolic. Black arrows indicate chosen values for velocity and anisotropy measurements

Phase Velocity Measurements

Figure 4 shows compressional wave velocities as a function of uniaxial stress (overburden pressure) in all measured directions. Not surprisingly, P wave velocity increased with pressure in all directions. This is due to a gradual closure of space between layers in the model. P-Wave velocity in the Z direction is significantly lower than in X and Y direction due to laminate finishing of the phenolic model used. Diagonal P-Wave measurements also show an overall increase with stress. Figure 4a shows phase velocities in ZX (25.4^0), ZY (45^0) and XY (26.6^0) as it varies with stress.

Shear wave splitting was observed and recorded in all principal direction during the course of the experiment.

Uniaxial stress and anisotropy

Fast and slow shear wave arrivals were picked and inverted stiffness coefficients and anisotropic parameters. Figure 5 displays a scaled shear wave seismogram as a function of polarization angle (0^0 to 180^0 every 10^0) in 3 different stress systems (0.16MPa, 0.33MPa and 0.52MPa). Signal scaling factor is 1:10000. Notice the decrease in arrival time for both fast (S1) and slow (S2) shear waves as stress increases. Figure 6 is a plot of fast and slow shear wave velocities as uniaxial stress increases.

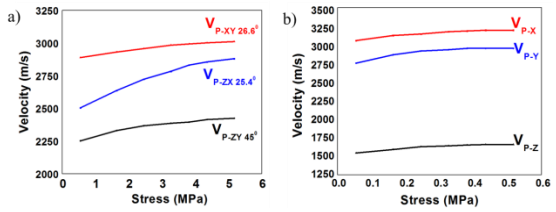

Figure 4: Compressional wave velocities as function of uniaxial stress in all measured directions. (P-wave velocity uncertainty is ± 0.15%)

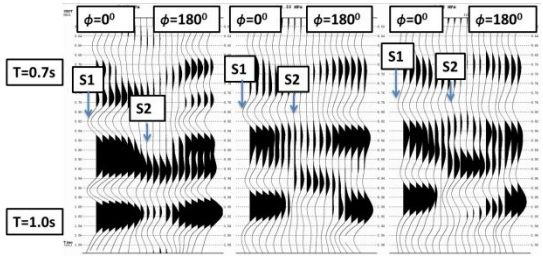

Figure 5: Shear wave seismogram, as a function of shear wave polarization (ϕ) in different stress regime (from left 0.16MPa, 0.33MPa and 0.52MPa)

It can be observed from Figure 6 that velocities of fast and slow shear waves largely increase with uniaxial stress. Also, the delay between fast and slow shear waves tends to generally diminish in all planes of measurement. However, in the Z direction, delay between fast and slow shear waves approaches a minimum; this is diagnostic of polar anisotropy (VTI). In a polar anisotropy (specifically VTI symmetry) case, $V_{s1(z)} = V_{s2(z)}$ because only one axis of symmetry exists.

Stiffness Coefficients

Elastic constants were derived from density and velocity measurements. P wave dependent stiffness coefficients were computed using the following equation,

$$C_{11} = \rho V p(x)^2 \quad (1)$$

Coefficients C_{22} *and* C_{33} were computed using similar equations according to their corresponding principal axes. Conversely, shear wave dependent elastic constants were calculated using Tsvankin (1997) extension of Thomsen's equation for orthorhombic models. In this case, it manifests as an averaging of fast and slow shear wave velocities across adjacent axes according to the following equation,

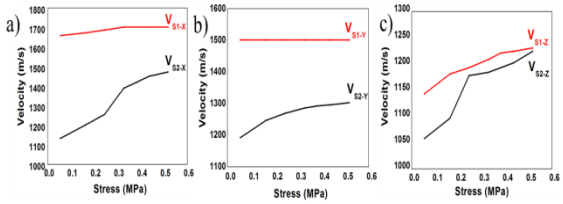

Figure 6: Fast and slow shear wave velocities in X (1), Y (2) and Z (3) direction as a function of uniaxial stress. (S-wave velocity uncertainty is ± 0.3%)

$$C_{44} = \rho \left(\frac{V_{s2(y)} + V_{s2(z)}}{2}\right)^2 \quad (2)$$

We also calculated C_{55} *and* C_{66} using similar approximations. Diagonal stiffness coefficients however were computed using a polar anisotropy assumption in each block face (or principal axis). Unambiguously VTI assumption in ZX and ZY axes and HTI in XY plane. Bearing in mind that we do not have exact 45^0 angles in some diagonal measurements, we have used an angle dependent form of Thomsen's (1986) equation and this eventually collapses to the more common diagonal elastic constant equations at 45^0 angles,

$$C_{13} = \left[\frac{A-B}{4\sin^2\theta\cos^2\theta}\right]^{0.5} - C_{44} \quad (3)$$

Where,

$$A = [2\rho V p_{zx}^2 - (C_{11} + C_{44})\sin^2\theta - (C_{33} + C_{44})\cos^2\theta\,]^2 \quad (3a)$$

$$B = [(C_{11} - C_{44})\sin^2\theta - (C_{33} - C_{44})\cos^2\theta\,]^2 \quad (3b)$$

The equation generally decomposes to the following when $\theta = 45^0$,

$$C_{13} = \left[\frac{\left(4Vp45(zx)^2 - C_{11} - C_{33} - 2C_{44}\right)^2 - (C_{11} - C_{33})^2}{4}\right]^{0.5} - C_{44} \quad (4)$$

Similar assumptions were used to calculate C_{23} *and* C_{12} (HTI approximation was used for C_{12}). Figure 7 shows compressional and shear wave dependent as well as diagonal stiffness coefficients as a function of uniaxial stress. Once again C_{33} is low (Figure 7a) in comparison to the rest due to the nature of the phenolic material being used.

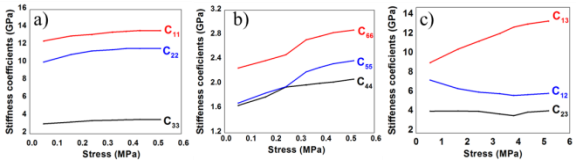

Figure 7: Stiffness coefficients as a function of uniaxial stress

Generally, within the limit of this experiment, all stiffness coefficients tend to increase with uniaxial stress (except C_{12} *and* C_{23} that tend to remain constant). Diagonal elastic constants (specifically C_{12} *and* C_{23}) remain largely constant with changing stress but C_{13} increases significantly with stress. This may be due to an unknown preferred orientation within the wave fabric of the phenolic model.

Anisotropic Parameters

In order to quantify the anisotropy in our measurements, anisotropic parameters γ *and* ε were computed using the same extension of Thomsen's parameter (Tsvankin, 1997). The equations are listed as the following,

$$\varepsilon_{xz} = \frac{1}{2}\left(\frac{V_{px}-V_{pz}}{V_{pz}}\right) = \varepsilon^1 \quad (5)$$

$$\gamma_x = \frac{1}{2}\left(\frac{Vs1(x)^2}{Vs2(x)^2} - 1\right) = \gamma^1 \quad (6)$$

Some earlier publications on orthorhombic anisotropy expressed these equations as ε^1 *and* γ^1. Figure 8 shows compressional (ε) and shear wave (γ) anisotropies as a function of uniaxial stress. Anisotropic parameter ε (Figure 8a) tends to remain constant in the limit of the experiment. The reason for the difference in ε_{yx} value is once more due to the nature of the composite phenolic material in the Z (or 3) direction. There is a large difference in compressional wave velocity in X or Y direction compared to Z which explains the large values of ε_{xz} *and* ε_{yz} compared to ε_{yx}. Anisotropic parameter γ (Figure 8b) largely diminishes with increasing stress. In the Z direction (γ_z) it tends towards zero at higher stress states. This is once again diagnostic of VTI symmetry. In a VTI polar anisotropy case, $\gamma_z = 0$

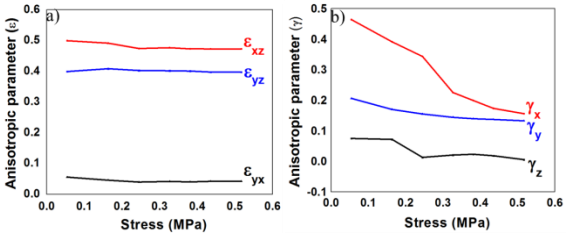

Figure 8: Anisotropic parameter ε (Compressional wave anisotropy) and γ (shear wave anisotropy) as a function of uniaxial stress

Conclusion

This experimental study has investigated changes in anisotropic parameters and stiffness coefficients in an orthorhombic medium as function of uniaxial stress. Results show that polar anisotropy (specifically VTI) symmetry appear to dominate the character of anisotropy in the Z (or 3) direction as uniaxial stress increases. This is particularly significant because this direction represents the direction normal to stratification and the plane of most interest to exploration geophysics. However, the orthotropic nature of the composite is revealed in other directions.

Acknowledgements

This physical modeling project was made possible by the financial support of Allied Geophysical Laboratories, University of Houston. The authors are grateful to Dr. Leon Thomsen and Dr. Evgeny Chesnokov for expert advice; Dr. Robert Wiley and Anoop William are also thanked for their help during the experiment

EDITED REFERENCES

Note: This reference list is a copy-edited version of the reference list submitted by the author. Reference lists for the 2011 SEG Technical Program Expanded Abstracts have been copy edited so that references provided with the online metadata for each paper will achieve a high degree of linking to cited sources that appear on the Web.

REFERENCES

Cheadle, S., J. Brown, and D. Lawton, 1991, Orthorhombic anisotropy: A physical seismic modeling study: Geophysics, **56**, 1603–1613, doi:10.1190/1.1442971.

Dellinger, J., and L. Vernik, 1994, Do traveltimes in pulse-transmission experiments yield anisotropic group or phase velocities?: Geophysics, **59**, 1774–1779, doi:10.1190/1.1443564.

Ebrom, D., J. A. McDonald, 1994, Seismic physical modeling: SEG Geophysics Reprint Series.

Pervukhina, M., D. Dewhurst, B. Gurevich, U. Kuila, T. Siggins, M. Raven, and H. M. N. Bolås, 2008, Stress-dependent elastic properties of shales: Measurement and modeling: The Leading Edge, **27**, 772–779, doi:10.1190/1.2944164.

Thomsen, L., 1986, Weak elastic anisotropy: Geophysics, **51**, 1954–1966, doi:10.1190/1.1442051.

Tsvankin, I., 1997, Anisotropic parameters and P-wave velocity for orthorhombic media: Geophysics, **62**, 1292–1309, doi:10.1190/1.1444231.